Spectrochimica Acta Part A: Molecular and Biomolecular Spectroscopy 322 (2024) 124772

Contents lists available at ScienceDirect

Spectrochimica Acta Part A:
Molecular and Biomolecular Spectroscopy

journal homepage: www.journals.elsevier.com/spectrochimica-acta-part-a-molecular-and-biomolecular-spectroscopy

Dimeric and monomeric conformation of SARS-CoV-2 main protease: New technical approaches based on IR radiation

Federica Piccirilli [a], Hendrik Vondracek [b,1], Lucia Silvestrini [c,2], Pietro Parisse [b,f], Francesco Spinozzi [c], Lisa Vaccari [b], Andrea Toma [d], Vincenzo Aglieri [d], Loredana Casalis [b], Antonio Palumbo Piccionello [e], Paolo Mariani [c], Giovanni Birarda [b,*], Maria Grazia Ortore [c,*]

[a] AREA Science Park, Padriciano 99, Trieste, I- 34149, Italy
[b] Elettra-Synchrotron Trieste S.C.p.A., Strada Statale 14, Basovizza, Trieste, I-34149, Italy
[c] Department of Life and Environmental Sciences, Marche Polytechnic University, via brecce bianche, Ancona, I-60131, Italy
[d] Fondazione Istituto Italiano di Tecnologia, via Morego 30, Genova, I- 16163, Italy
[e] Dipartimento di Scienze e Tecnologie Biologiche Chimiche e Farmaceutiche, viale delle scienze, Palermo, I-90133, Italy
[f] CNR - Istituto Officina dei Materiali, s.s. 14 km 163.5 in Area Science Park, 34149 Basovizza, Trieste, Italy

GRAPHICAL ABSTRACT

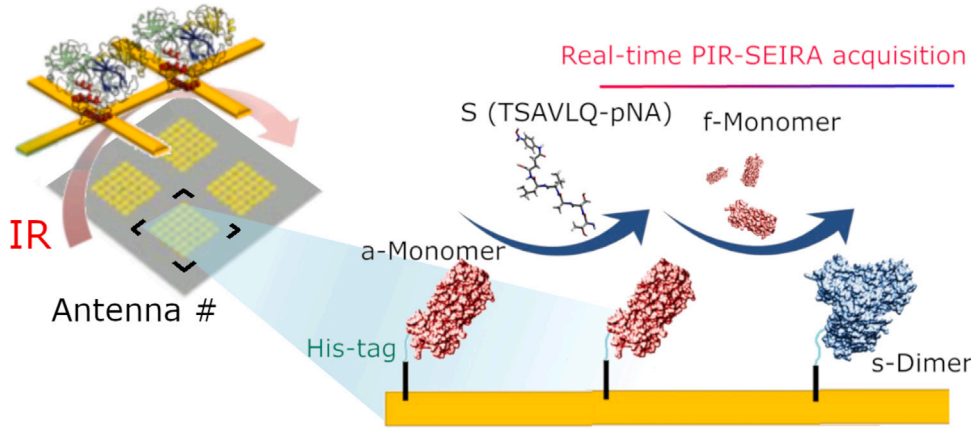

HIGHLIGHTS

- Direct evidence of M^{pro} substrate-mediated dimerization through IR probe.
- Secondary structure evaluation of M^{pro} monomers and dimers.
- Short intermolecular β-sheet stabilize M^{pro} dimers.

ARTICLE INFO

Keywords:
IR

ABSTRACT

The main proteases M^{pro} are a group of highly conserved cysteine hydrolases in β-coronaviruses. They have been demonstrated to play an unavoidable role in viral replication, and consequently they have

* Corresponding authors.
E-mail addresses: giovanni.birarda@elettra.eu (G. Birarda), m.g.ortore@univpm.it (M.G. Ortore).
[1] Now at Diamond Light Source, MIRIAM Infrared Beamline B22, Harwell Science and Innovation Campus, Didcot, United Kingdom.
[2] Now at Università Vita-Salute San Raffaele, Laboratorio di Microbiologia e Virologia, Milano, and at Operations - Research and Development, DGforLife, Marcallo con Casone, Milano, Italy.

https://doi.org/10.1016/j.saa.2024.124772
Received 31 March 2024; Received in revised form 11 June 2024; Accepted 2 July 2024
Available online 6 July 2024

SARS-COV2
Protease
Equilibria

been suggested as key targets for treating coronavirus-caused infectious diseases, mainly from the COVID-19 epidemic. Since the most functional form for M^{pro} enzymatic activity is associated to its homodimer, compounds inhibiting dimerization should also inhibit catalytic activity. We show how PIR-SEIRA (Plasmonic Internal Reflection-Surface Enhanced InfraRed Absorption) spectroscopy can be a noteworthy technique to study proteins subtle structural variations associated to inhibitor binding. Nanoantennas arrays can selectively confine and enhance electromagnetic field via localized plasmonic resonances, thus promoting ultrasensitive detection of biomolecules in close proximity of nanoantenna arrays and enabling the effective investigation of protein monolayers. By adopting this approach, reflection measurements conducted under back illumination of nanoantennas allow to probe anchored protein monolayers, with minimum contribution of environmental buffer molecules. PIR-SEIRA spectroscopy on M^{pro} was carried out by *ad hoc* designed devices, resonating in the spectral region of Amide I and Amide II bands. We evaluated here the structure of anchored monomers and dimers in different buffered environment and in presence of a newly designed M^{pro} inhibitor. Experimental results show that dimerization is not associated to relevant backbone rearrangements of the protein at secondary structure level, and even if the compound inhibits the dimerization, it is not effective at breaking preformed dimers.

1. Introduction

In recent years, there has been a significant amount of research conducted on SARS-CoV-2, the positive-stranded RNA coronavirus that has caused the Covid-19 pandemic. The replicase gene encodes two overlapping polyproteins, predominantly processed by the main protease (M^{pro}). This crucial enzyme emerged as a highly promising candidate for therapeutic purposes and indeed proved to be a successful target for anti-SARS-CoV-2 drug development [1,2]. t [1]. Given that the functional form of M^{pro} has always been regarded as dimeric, compounds that interfere with dimerization should theoretically reduce its catalytic activity. However, the compound-induced shift of the dimer-monomer equilibrium does not directly translate into a loss of enzymatic activity. Indeed, the latter strongly depends also on the local interactions occurring at the catalytic site, which in turn rules the competition between inhibitor and substrate. In light of this discovery, it appears very important to better understand the conformational differences of M^{pro} induced by dimerization, and to evidence changes induced by the most efficient compounds arising from previous work [1]. In fact, several PDB entries related to M^{pro}, alone and/or complexed with drugs, have been published in the last years, including a new-inactive conformation [3] where a new cavity is present, and the N-terminal and C-terminal tails, as well as the dimeric interface, are perturbed with a subsequent destabilization of the dimer. These recent results suggest the importance to further investigate M^{pro} conformations and their relationship with activity.

The investigation into the monomer–dimer equilibrium in proteins is not confined to the case of M^{pro}. There are several comparable cases where the association and activity properties of proteins are intimately linked [4–8]. Dimeric proteins may form through the exchange of structural domains between monomers, although the prevalence of this phenomenon remains unclear. The mechanism whereby identical proteins swap reciprocal segments to create dimers is commonly known as domain swapping, and induced domain swapping (INDOS) can indeed serve as a mechanism for regulating protein function [9]. However, at the moment there is no experimental technique of election that allows studying homodimerization in solution. The lack of accurate measurements make it challenging to precisely determine the equilibrium constant of dimer dissociation. Consequently, the possibility to isolate monomers and dimers, and to investigate their propensity to bind to a specific drug, can be of high interest, even for pharmaceutical purposes.

Among all the techniques addressing the secondary structure of proteins, infrared spectroscopy stands out for its versatility and chemical sensitivity. Fourier transform infrared spectroscopy (FTIR) allows the determination of protein secondary structure through the analysis of the Amide I band (1580–1710 cm^{-1}), that is mostly associated to the C=O stretching vibration. Amide I is indeed extremely sensitive to protein secondary structural elements since the carbonyl stretching vibrational energy depends on the specific hydrogen-bonding network in helices, sheets, turns and unordered structural elements. Through infrared spectroscopy (FTIR) it is thus possible to define proteins secondary structure from Amide I deconvolution into its overlapping components. Surface Enhanced Infrared Absorption spectroscopy (SEIRA), coupled with Plasmonic Internal Reflection detection (PIR-SEIRA), represents an innovative surface-based optical technique that has significantly improve infrared spectroscopy sensitivity to the molecular level and offers at the same time the capability of working in hydrated conditions. The method relies on exploiting plasmonic effects for the spatial confinement and enhancement of electromagnetic radiation at the nanoscale [10]. Specifically, PIR-SEIRA can be finely tuned through the design of customized structures, enabling the study of single protein monolayers under precise environmental conditions. The antennas are fabricated onto a IR transparent substrate, generally CaF_2, and in PIR geometry the substrate is back illuminated. The light passing through the substrate is confined and back-scattered by the antenna. It is then internally reflected and partly absorbed by the molecules in proximity to the surface. PIR-SEIRA provides thus the chance to investigate samples at the nanoantenna surface in solution, without worrying about path length, as in the ATR technique, since the effective interaction is entirely determined by the penetration depth of the evanescent wave within the sample. Static conditions, with proteins in buffered environment, can indeed be probed as well as dynamic environmental states involving protein-ligand interactions. Nevertheless its application remains predominantly limited to model systems as proof of principle demonstrations. To date, only a handful of articles have been published showcasing the technique's potential in yielding insights into real systems [10].

In this paper, we exploit PIR-SEIRA to investigate the M^{pro} dimerization equilibrium in the presence of ligand molecules. Specifically, our focus is on M^{pro} substrate-mediated dimerization triggered by TSAVLQ-pNA [11]. and the effects on M^{pro} dimer induced by the presence of an inhibitor. Specifically, inhibitor **NV1399** investigated by Silvestrini et al. [1] and referred to as compound **7**, was selected. It is noteworthy that, among all the inhibitors examined by Silvestrini et al. inhibitor **NV1399** (**7**) stands out for its ability to simultaneously inhibit the enzymatic activity of M^{pro} while producing the most pronounced effect in dimer dissociation. Indeed, it has been shown that, in the presence of 60 μM of inhibitor **NV1399**, the dissociation equilibrium constant (K_D) of the M^{pro} dimer increases up to 30 ± 10 μM, compared to 7±1 μM in the absence of the inhibitor. With the presented experiments we propose PIR-SEIRA as a robust method for exploring the intricate structure-function relationships within proteins. While this investigation primarily focuses on a specific structural alteration produced by a ligand, in light of its impact on the enzymatic activity of M^{pro}, it paves the way for the future application of this technique to a broader range of inhibitors.

2. Materials and methods

2.1. M^{pro} expression, purification, and his-tag cleavage

SARS-CoV-2 Main protease (M^{pro} $NC_0045512$) was produced by a recombinant strain of *E. coli*, BL21DE3pLys, harboring a pET28-based M^{pro} expressing vector. The protein was synthesized with an N-terminal HIS-tag, which can be removed through thrombin digestion using the Thrombin CleanCleaveTM kit from Merck. *E. coli* recombinant strain was grown on LB medium containing 50 μg/ml Kanamycin and 34 μg/ml Chloramphenicol as selective antibiotics. Cultures were grown up to OD600 (Optical Density at 600 nm wavelength) of 0.6 – 0.8 at 37 °C, 200 rpm and then M^{pro} expression was induced by addition of 0.5 mM isopropyl-1-thio-β-D-galactopyranoside (IPTG). Growth was achieved for 3 h at 37 °C and then cells were harvested by centrifugation at 6000 g. Pellets were re-suspended in lysis buffer (20 mM Tris-HCl, pH 8.0, 300 mM NaCl, 2 mM β-mercaptoethanol) for total extract. Cell rupture was achieved by sonication (Sonics Vibra Cell sonicator) at 4 °C. Cell debris was separated from the total protein extract by centrifugation at 6500 g for 1 h. Clarified cell extract was loaded onto Ni-NTA affinity column (G-Biosciences) and washed by washing buffer (Tris-HCl 20 mM, pH 7.6, NaCl 100 mM). M^{pro} was eluted from the column by 3 column volumes of elution buffer (Tris-HCl 20 mM, pH 7.6, NaCl 100 mM, imidazole 300 mM). The collected samples were loaded onto 12% SDS-PAGE and the fraction containing M^{pro} was treated for thrombin cleavage of HIS-tag when required for experimental purpose. Treated and un-treated thrombin M^{pro} samples were loaded in separated experimental sessions to ÄKTA Fast Protein Liquid Chromatography (FPLC) to obtain purified M^{pro} with and without HIS-tag. The purified protein was quantified by OD at 280 nm.

2.2. Proteins anchoring on plasmonic devices

Plasmonic devices have been fabricated on CaF_2 substrate. Every device is composed by 24 micro-patterned arrays (or fields) having a size of 50 × 50 mm (see Fig. 1a), each consisting of a gold nanoantenna matrix with cross-shaped geometry, specifically designed for enhancing both p- and s-polarized IR light in the spectral region of protein Amides (i.e. 1420−1820 cm^{-1}). Further details on the device design and fabrication can be found in [10]. The protein anchoring onto the nanoantennas followed the His-tag binding method previously developed [12], with minor modifications. In brief, the nanoantennas were incubated in 500 μl of a solution of 15 μM thiolated Nitrilotriacetic Acid (NTA) in ethanol for at least 6 h at 4 °C. The surface was then repeatedly washed with buffer (Tris-HCl 20 mM, pH 7.6, NaCl 100 mM), and incubated for 10 min with 500 μl of EDTA 500 mM, pH 8.6, to remove residual metal ions. After washing with ultra-pure water, the plasmonic device was incubated with 500 μl of a 10 mM $CoCl_2$ solution in Tris-HCl buffer (pH 8.6, as before) for at least 6 h at 4 °C. Finally, the device was repeatedly washed with ultra-pure water and incubated with 355 μl of a solution of M^{pro} monomers 500 nM for 1 h. The functionality of the protocol was verified using Atomic Force Microscopy (AFM) nanografting. To this purpose, the anchoring protocol was applied on an ultra-flat Ulman-type gold surface. AFM images are shown in Figs. S1 of the Supplementary Materials (SM).

2.3. Dimerization treatment and inhibitor testing

To induce homo-dimerization, anchored M^{pro} monomers were pre-incubated with the colorimetry-based peptide substrate TSAVLQ-para-nitroanilide (TSAVLQ-pNA), known to favor dimerization [13], for 30 min at 36 °C. This methodology will henceforth be referred to as substrate-mediated dimerization [13]. Subsequently, the device's surface was repeatedly washed and then subjected to incubation with other monomers in solution (500 nM, in Tris-HCl buffer pH 8.6) for 30 min. PIR-SEIRA real-time measurements were performed to monitor the formation of dimers during this second incubation phase. The effect of the inhibitor **NV1399** that was obtained as previously reported [1], has been then tested by following two different procedures, aimed at probing its impact alternatively on dimers or on monomers. In these second set of experiments all PIR-SEIRA spectra were acquired under static conditions in buffer, i.e. at the end of the each incubation step upon extensive washing in order to remove residual unbound molecules. To test the effect of inhibitor **NV1399** on dimers, the anchored monomeric monolayer (Step 1 of Fig. 2) was subjected to the substrate-mediated dimerization method described above (Step 2 of Fig. 2). Subsequently, the dimer was incubated with the inhibitor **NV1399** for 10 min (Step 3 of Fig. 2). In the second procedure, aimed at probing the effect of inhibitor **NV1399** on monomers, anchored monomers (Step 1 of Fig. 3) were first incubated with TSAVLQ-pNA substrate for 30 min, then with inhibitor **NV1399** for 10 min. Subsequently, the monolayer was incubated with a solution containing M^{pro} monomers incubated with inhibitor **NV1399**. PIR-SEIRA spectra were then acquired upon extensive device's surface washing (Step 2 of Fig. 3).

2.4. SEIRA measurements and data analysis

The infrared measurements were conducted at the Chemical and Life Sciences branch of SISSI beamline (SISSI-Bio) at Elettra Synchrotron (Trieste, Italy) [14]. We adopted the PIR-SEIRA approach [15], with functionalized arrays mounted in upside down configuration within a fluidic cell, as described in [10]. Spectral acquisition was performed with the Bruker Hyperion 3000 IR-Vis microscope coupled to a Bruker Vertex 70v interferometer and equipped with a HgCdTe detector. Measurements were performed in reflection mode using a 15× Schwarzschild objective, with a knife-edge aperture set to 50 × 50 μm^2 to collect data from individual plasmonic arrays (see Fig. 1a). The acquired spectral range was between 800 and 4000 cm^{-1}, with a spectral resolution of 4 cm^{-1} at 40 kHz scanner velocity. 512 scans were accumulated and averaged for each single measurement. Fourier transform was carried out with Mertz phase gicorrection, using a Blackman–Harris 3-terms apodization function. Background spectra were repeatedly collected after the measurement of three device arrays on a golden patch specifically fabricated for this purpose. This procedure ensured that identical experimental conditions were maintained for both sample and background measurements. Subtracted spectra were cut between 1500–1750 cm^{-1}, averaged (5 fields were used for each average) and baseline corrected. The vector normalized second derivatives were computed (Savitzky–Golay filter, 17 smoothing points) in the region of interest using OPUS 8.5 software routines.

3. Results and discussion

In a recent work, compound **NV1399** (also identified as compound **7**) had been demonstrated to have an inhibiting effect on M^{pro}, whose strength is proportional to its capability to induce the dissociation of the M^{pro} dimer, in comparison with other compounds [1]. Compound **NV1399** interacts with two residues of the S1, Leu141 and Glu166. The binding with Glu166 should be via an hydrogen bond, and could be linked to its high inhibiting action. In order to study M^{pro} conformations changes induced by this compound, we took advantage of the high sensitivity of PIR-SEIRA in providing direct evidence of proteins backbone arrangement, in terms of secondary structure. For these experiments we utilized the experimental setup outlined in [10]. Our SEIRA devices were designed to enhance a specific spectral region thanks to a cross-shaped gold pattern motif resonating in the spectral region around 1600 cm^{-1}. Such designed system allows to confine and enhance both p- and s- polarized IR light into a small volume in proximity of the gold pattern (in the range of up to tens of nm). The specificity of the device for probing proteins conformations relies in

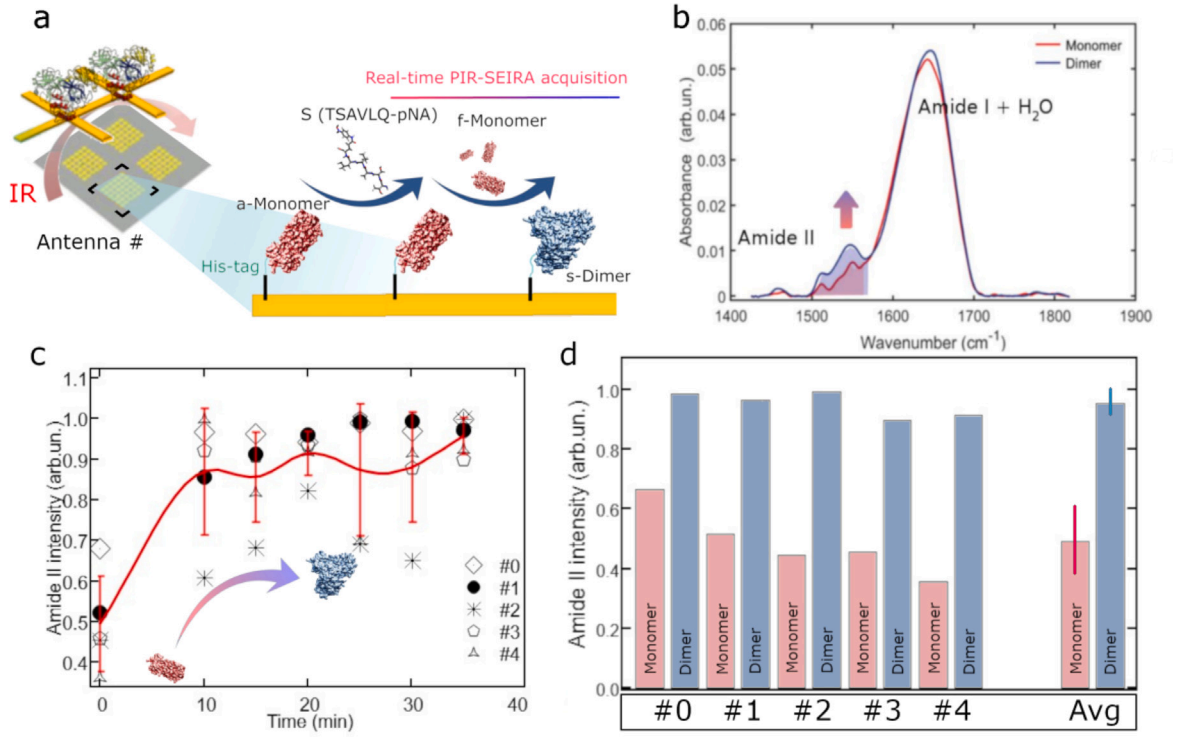

Fig. 1. (a) Scheme of PIR-SEIRA acquisition with M^{pro} monolayer anchored to the gold nanoantennas SH-NTA functionalized array and IR illumination of each nanoantenna array from the backside, following PIR detection scheme. The pattern describing the substrate-assisted dimerization of M^{pro} through the binding of M^{pro} monomers in solution is shown; (b) IR absorbance spectra, averaged over 5 arrays obtained from M^{pro} monomers and dimers in solution as initial and final state of substrate assisted dimerization; (c) time evolution of Amide II intensity during the dimerization process. The signal of each antenna array (from #0 to #4) is plotted with markers. The tendency curve built on average values is shown as a red line, with standard deviations calculated at each experimental time point. (d) Intensity of Amide II band for both the initial (monomers, in red) and final (dimers, in blue) sample conditions calculated for each antenna (from #0 to #4). Average values (Avg) are also shown with standard deviation.

the matching of the resonance of the nanoantenna arrays with Amide I and Amide II bands of proteins, that will be thus selectively amplified. Before conducting PIR-SEIRA analysis, we designed and optimized the anchoring process as described in [16]. The efficacy of the anchoring was tested through in solution AFM measurements (Fig. S1 of the SM) on functionalized nanografted gold-substrate. According to AFM measurements, the height of the protein monolayer anchored to the gold surface is in average of 3.6 ± 0.3 nm with a roughness (root-mean square, RMS) of 1.6 ± 0.3 nm. The high RMS value, constituting 48% of the average height, indicates heterogeneity within the monolayer, potentially due to proteins adopting various orientations relative to the functionalized surface. The optimum protocol was then applied to the SEIRA substrates to allow for infrared analysis on anchored M^{pro} monomers and dimers.

A first set of experiments was aimed at demonstrating the efficacy of the technique in detecting the anchoring of M^{pro} monomers and the substrate-assisted formation of dimers (see Fig. 1a). As sketched in Fig. 1a, we first measured the spectrum of anchored monomers (henceforth, a-monomers). a-Monomers were then subjected to two steps of treatment: firstly, they were incubated with a solution containing the substrate molecule TSAVLQ-pNA favoring dimerization [13], then incubated with free M^{pro} monomers in solution (henceforth, f-monomers), to form the dimer (s-dimer). Fig. 1b shows the comparison of M^{pro} PIR-SEIRA absorption spectra before and after the substrate-assisted dimerization. Both spectra show a prominent peak centered around 1640 cm^{-1}, due to the overlapping of OH bending mode of water and the Amide I band of M^{pro}, with a shoulder at about 1550 cm^{-1}, related to the Amide II band of M^{pro}. Indeed, as discussed in [15], PIR-SEIRA spectroscopy enhances the absorption of the molecules located in close proximity of the nanoantennas, by taking advantage of the extremely confined interaction associated with near-field/evanescent wave localization, and the penetration depth of the IR probing light is in the length scale of few tens of nm and depends on antenna topology [10]. More specifically, when protein monolayers in buffer solution are measured, the PIR-SEIRA spectrum contains the signal of the anchored proteins plus the contribution of the adjoining buffer molecules, with an extent of the latter that depends, in addition to the coverage, on the size of the specific protein. In particular, since the penetration depth of signal in the PIR-SEIRA devices used in the preset study is of tens of nm [10], and being the thickness of the M^{pro} monolayer of only few nm, a consistent contribution of water absorption to the spectra was expected. Given the overlapping of Amide I band to OH bending of water, to probe f-monomers binding to the monolayer, we focused on the evolution of Amide II band, that is less affected by water absorption contributions.

Fig. 1c illustrates the kinetic evolution of the Amide II peak intensity detected for 5 fields. On average, it is observed that the Amide II peak intensity essentially doubles after approximately 10-15 min, reaching a plateau thereafter. However, as shown in Fig. 1d, the absolute values of Amide II absorbance at both initial and final states depend on the specific array, with the intensity at the final state being, on average, and for most of the antennas, around twice the initial one. In order to strengthen this interpretation and clearly define the merit and the limit of the procedure in interpreting the Amide II band variation observed, we performed three independent dimerization experiments exploiting three distinct batches of antennas, with the same expected performances. Upon comparing the three experiments (See Fig S2 of the SM), it is evident that while both protein and water signals exhibit dependence on the specific batch, the Amide II intensity upon dimerization is between 1.5 and 2 times the initial one. Ideally, the formation of dimers should be accompanied by a doubling of the Amide II intensity. The slight deviation from the ideal case can be attributed to several factors, including the presence of defects in the monolayer, slight geometrical variations in gold patterning, and possible degradation of

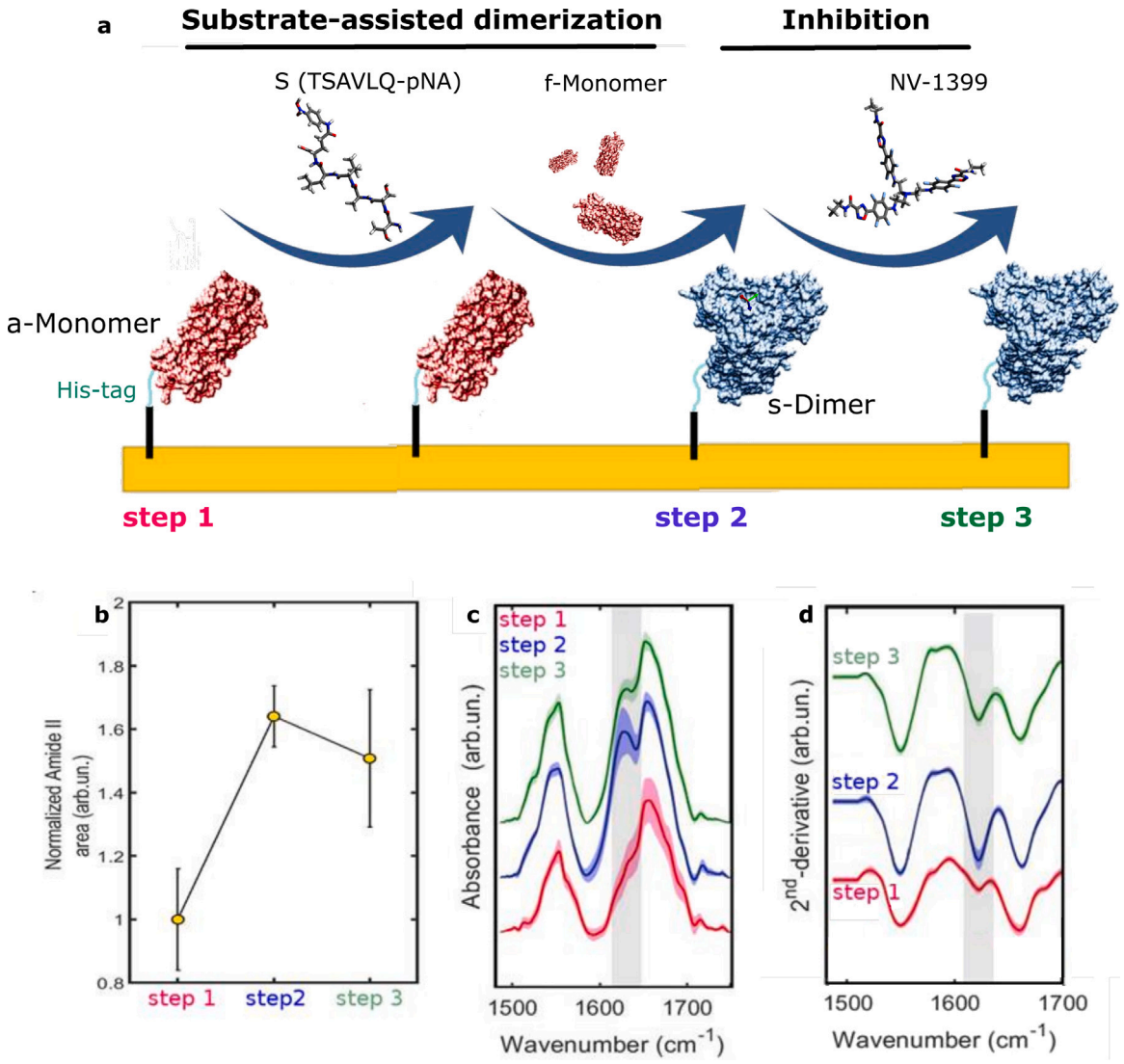

Fig. 2. Effect of Inhibitor **NV1399** on M^{pro} anchored dimers formed through the substrate-assisted methodology. (a) Schematic representation of sample during the treatment. Step 1: untreated a-monomer; step 2: s-dimer (obtained through substrate-assisted dimerization); step 3: s-dimer after incubation with inhibitor **NV1399**. (b) Normalized Amide II area as obtained for each step previously described. (c) Buffer subtracted absorption spectra. (d) 2nd-derivative of spectra in the region of Amide I (1580–1710 cm^{-1}) and Amide II (1480–1580 cm^{-1}) bands. The gray area highlights the spectral region where the main spectral changes occur on Amide I during the process.

antennas due to repeated use, among others. Indeed, the combination of these factors collectively contributes to lowering the intensity of Amides and/or unbalancing the relative intensity of water and protein signals.

The effects that the inhibitor **NV1399** exerted on both a-monomers and s-dimers, were then tested with PIR-SEIRA. The experimental approach and the results of these experiments are summarized in Figs. 2 and 3. a-Monomers dimerization was induced by TSAVLQ-pNA substrate as for the experiments shown in Fig. 1. The monolayer was hence incubated with a solution containing the inhibitor **NV1399** in excess, at 480μM. The untreated monomers were identified as the Step 1 of the experiment, the dimers as the Step 2, and the s-dimer incubated with inhibitor **NV1399** as the step 3. The values of the Amide II band area at the three steps of the experiment are compared in Fig. 2b. While the increase in the Amide II area from Step 1 to Step 2 aligns with previous results, it is notable that after incubating s-dimers with inhibitor **NV1399**, no statistically significant changes are observed. This suggests minimal or no interaction of inhibitor **NV1399** with the anchored dimers. To evaluate possible changes in the secondary structure of M^{pro} dimers, the Amide I band was considered. The buffer-subtracted absorbance spectra of a-monomer (Step 1), of substrate-assisted s-dimer (Step 2) and of s-dimer in the presence of inhibitor **NV1399** are plotted in Fig. 2c, as red, blue and green curves respectively. Second derivative of the same spectra are plotted in Fig. 2d, maintaining the same color code. The plotted spectra are the average of 5 measurements and the shadowed region represents the standard deviation of the measurements. As it can be observed from Fig. 2c, the Amide I of the a-monomer at Step 1 has a main peak at 1660 cm^{-1}, associated to the α-helix moieties of M^{pro}, with a minor contribution at 1636 cm^{-1}. The aforementioned contribution to the Amide I band became notably more pronounced for s-dimers at Step 2 and Step 3. This peak can be linked to the structural β-sheets present in monomers, and its increase may result from the formation of short intermolecular β-sheets, potentially stabilizing dimeric M^{pro} [17–19]. In support to this data interpretation, anti-parallel β-sheet has been observed for M^{pro} of SARS-Cov-1 at the substrate binding site [20]. The incubation with inhibitor **NV1399** produces no changes in the Amide I 2nd-derivative spectrum but a subtle reduction of the minimum at 1636 cm^{-1}. This reduction of β-sheet signal occurs together with a reduction of Amide II intensity. Both the effects point at the slight

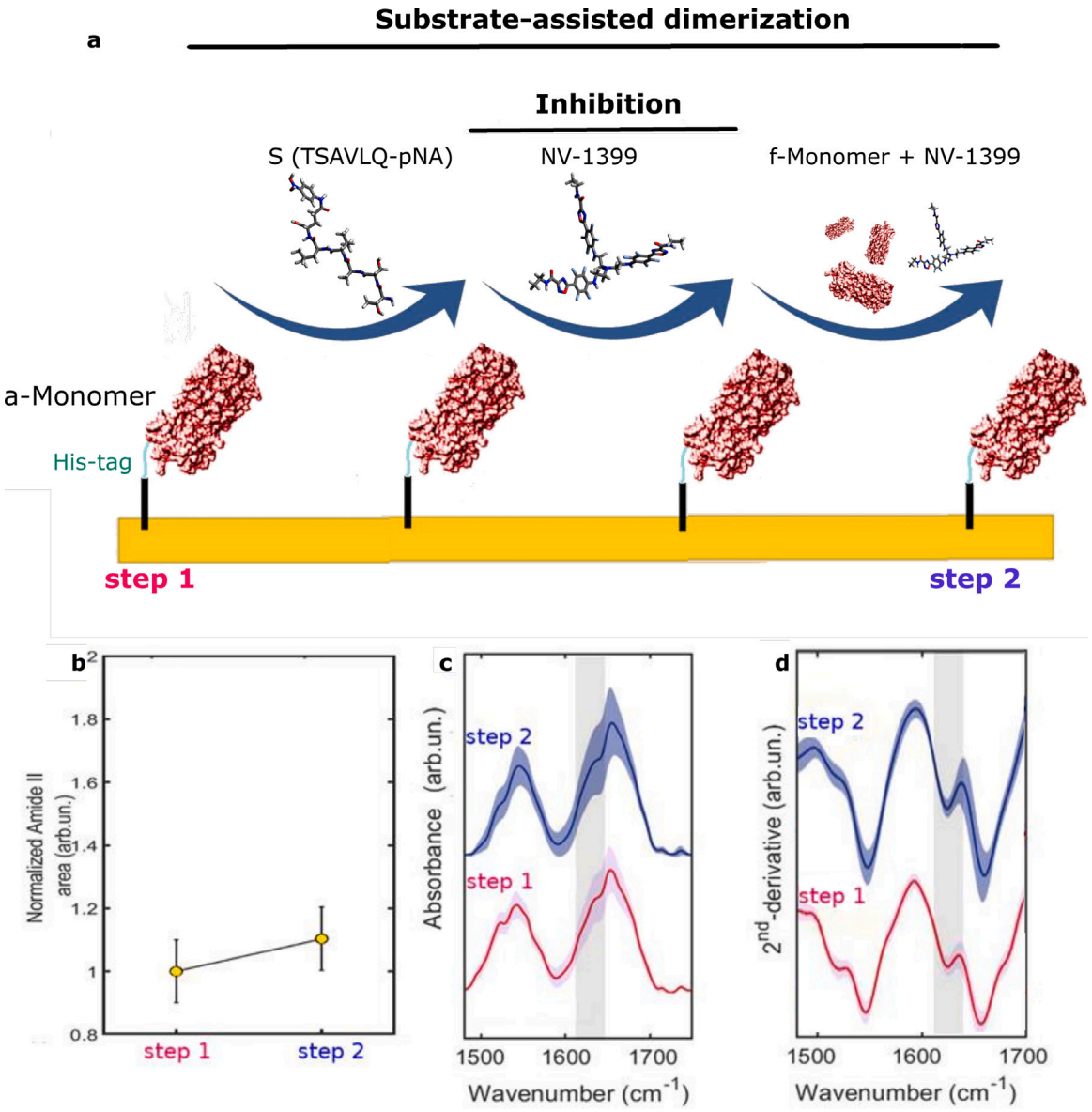

Fig. 3. (a) Substrate-mediated incubation of **NV1399**-treated a-monomers with **NV1399**-treated f-monomers. Two steps of treatment are shown, before and after incubation of **NV1399**-a-Monomers with **NV1399**-f-monomers. (b) Normalized Amide II area. (c) Buffer subtracted absorption spectra (d) and 2nd-derivative in the region of Amide I (1580–1710 cm^{-1}) and Amide II (1480–1580 cm^{-1}) bands. The gray area highlights the spectral region where the main spectral changes occur on Amide I during the process.

decrease of dimers extent upon inhibitor **NV1399** interaction. Further analyses aimed to probe the effect of inhibitor **NV1399** on the dimerization process were performed by incubating a-monomers (pretreated with dimer inducing substrate) with a solution containing a mixture of inhibitor **NV1399** and f-monomers. As suggested by the Amide II area calculated for a-monomers after incubation with inhibitor **NV1399** and at the end of the dimerization treatment, we did not observe any evidence of dimerization in this case (Fig. 3). From the observation of Amide I 2nd-derivative spectra, no changes are detected in secondary structure as well, being the second derivative profile more similar to Step 1 at Fig. 2d. From the results presented in Figs. 2 and 3, we can draw three main conclusions: (1) the inhibitor **NV1399** effectively blocks dimerization and (2) it has only a slight effect in dissociating preformed dimers; (3) the formation of dimers is accompanied by the stabilization of short intermolecular β-sheets.

4. Conclusion

This study shows the application of the PIR-SEIRA technique in understanding the formation and stability of the SARS-CoV-2 M^{pro} dimer. Unlike other methods, PIR-SEIRA technology allows for the accurate evaluation of dimer formation and stability starting from monomers anchored to a surface and in contact with the buffer solution containing free monomers. Our data provide insights into the effect of inhibitory compounds, with potential applications as antiviral drugs, on both preformed dimers and on the interaction between anchored and free monomers. This specific and detailed information, not accessible through other in-solution techniques such as SAXS or CD, adds an important element of knowledge regarding the molecular mechanism by which an inhibitor exerts its function. The extensive literature accumulated in recent years, coupled with the onset of the Covid-19 pandemic, has revealed that there is no single molecular mechanism of inhibition and that enzymatic inhibition is not necessarily correlated with the dissociation of the M^{pro} dimer, which is believed to be the enzymatically active form. In perspective, therefore, the innovative PIR-SEIRA technique may be systematically applied to different inhibitors of M^{pro} (or other biological active homodimers), providing a further valuable piece of knowledge against the SARS-CoV-2, or eventually other, viral infection.

CRediT authorship contribution statement

Federica Piccirilli: Writing – original draft, Investigation, Conceptualization. **Hendrik Vondracek:** Investigation. **Lucia Silvestrini:** Investigation, Conceptualization. **Pietro Parisse:** Investigation. **Francesco Spinozzi:** Conceptualization. **Lisa Vaccari:** Supervision, Formal analysis. **Andrea Toma:** Methodology. **Vincenzo Aglieri:** Funding acquisition. **Loredana Casalis:** Supervision. **Antonio Palumbo Piccionello:** Resources. **Paolo Mariani:** Funding acquisition. **Giovanni Birarda:** Writing – original draft, Investigation, Conceptualization. **Maria Grazia Ortore:** Writing – original draft, Supervision, Conceptualization.

Declaration of competing interest

The authors declare that they have no known competing financial interests or personal relationships that could have appeared to influence the work reported in this paper.

Data availability

Data will be made available on request.

Acknowledgments

The authors acknowledge the CERIC-ERIC Consortium for the access to experimental facilities via the proposal 20202204. This work has been partially funded by the project Vitality – Project Code ECS0000041, CUP I33C22001330007 - funded under the National Recovery and Resilience Plan (NRRP), Mission 4 Component 2 Investment 1.5 - 'Creation and strengthening of innovation ecosystems,' construction of 'territorial leaders in R&D' – Innovation Ecosystems - Project 'Innovation, digitalization and sustainability for the diffused economy in Central Italy – VITALITY' Call for tender No. 3277 of 30/12/2021, and Concession Decree No. 0001057.23-06-2022 of Italian Ministry of University funded by the European Union – NextGenerationEU. This work has been partially funded by the project funded under the National Recovery and Resilience Plan (NRRP), Mission 4 Component 2 Investment 1.4 - Call for tender No. 3138 of 16 December 2021, rectified by Decree n.3175 of 18 December 2021 of Italian Ministry of University and Research funded by the European Union – NextGenerationEU; award Number: Project code CN_00000033, Concession Decree No. 1034 of 17 June 2022 adopted by the Italian Ministry of University and Research, CUP I33C22001300007 Project title "National Biodiversity Future Center - NBFC".

Appendix A. Supplementary data

Supplementary material related to this article can be found online at https://doi.org/10.1016/j.saa.2024.124772.

References

[1] L. Silvestrini, N. Belhaj, L. Comez, Y. Gerelli, A. Lauria, V. Libera, P. Mariani, P. Marzullo, M.G. Ortore, A. Palumbo Piccionello, C. Petrillo, L. Savini, A. Paciaroni, F. Spinozzi, The dimer-monomer equilibrium of SARS-CoV-2 main protease is affected by small molecule inhibitors, Sci. Rep. 11 (1) (2021) http://dx.doi.org/10.1038/s41598-021-88630-9.

[2] T. Kronenberger, S.A. Laufer, T. Pillaiyar, COVID-19 therapeutics: Small-molecule drug development targeting SARS-CoV-2 main protease, Drug Discov. Today 28 (6) (2023) 103579, http://dx.doi.org/10.1016/j.drudis.2023.103579.

[3] E. Fornasier, M.L. Macchia, G. Giachin, A. Sosic, M. Pavan, M. Sturlese, C. Salata, S. Moro, B. Gatto, M. Bellanda, R. Battistutta, A new inactive conformation of SARS-CoV-2 main protease, Acta Crystallogr. D 78 (3) (2022) 363–378, http://dx.doi.org/10.1107/S2059798322000948.

[4] M.G. Ortore, F. Spinozzi, C. Carsughi, P. Mariani, M. Bonetti, G. Onori, High pressure small-angle neutron scattering study of the aggregation state of beta-lactoglobulin in water and water / ethylene glycol solutions, Chem. Phys. Lett. 418 (2005) 338–342.

[5] D.S. Froese, T. Krojer, X. Wu, R. Shrestha, W. Kiyani, F. von Delft, R.A. Gravel, U. Oppermann, W.W. Yue, Structure of MMACHC reveals an arginine-rich pocket and a domain-swapped dimer for its B12 processing function, Biochemistry 51 (25) (2012) 5083–5090, http://dx.doi.org/10.1021/bi300150y.

[6] J.K. Keppler, D. Martin, V.M. Garamus, K. Schwarz, Differences in binding behavior of (-)-epigallocatechin gallate to ??-lactoglobulin heterodimers (AB) compared to homodimers (A) and (B), J. Mol. Recognit. 28 (11) (2015) 656–666, http://dx.doi.org/10.1002/jmr.2480.

[7] R. Passantino, M.R. Mangione, M.G. Ortore, M.A. Costa, A. Provenzano, H. Amenitsch, R. Sabbatella, C. Alfano, V. Martorana, S. Vilasi, Investigation on a MMACHC mutant from cblC disease: The c.394C>T variant, Biochim. Biophys. Acta 1870 (6) (2022) 140793, http://dx.doi.org/10.1016/j.bbapap.2022.140793, URL https://www.sciencedirect.com/science/article/pii/S1570963922000401.

[8] A. Teichmann, A. Gibert, A. Lampe, P. Grzesik, C. Rutz, J. Furkert, J. Schmoranzer, G. Krause, B. Wiesner, R. Schülein, The specific monomer/dimer equilibrium of the corticotropin-releasing factor receptor type 1 is established in the endoplasmic reticulum, J. Biol. Chem. 289 (35) (2014) 24250–24262, http://dx.doi.org/10.1074/jbc.M114.553644, URL https://www.sciencedirect.com/science/article/pii/S0021925820319633.

[9] J.M. Karchin, J. Ha, K.E. Namitz, M.S. Cosgrove, S.N. Loh, Small molecule-induced domain swapping as a mechanism for controlling protein function and assembly, Sci. Rep. 7 (2017) 44388, http://dx.doi.org/10.1038/srep44388.

[10] P. Zucchiatti, G. Birarda, A. Cerea, M.S. Semrau, A. Hubarevich, P. Storici, F. De Angelis, A. Toma, L. Vaccari, Binding of tyrosine kinase inhibitor to epidermal growth factor receptor: surface-enhanced infrared absorption microscopy reveals subtle protein secondary structure variations, Nanoscale 13 (2021) 7667–7677, http://dx.doi.org/10.1039/D0NR09200B.

[11] C.-G. Wu, S.-C. Cheng, S.-C. Chen, J.-Y. Li, Y.-H. Fang, Y.-H. Chen, C.-Y. Chou, Mechanism for controlling the monomer–dimer conversion of SARS coronavirus main protease, Acta Crystallogr. D 69 (5) (2013) 747–755, http://dx.doi.org/10.1107/S0907444913001315.

[12] B. Sanavio, D. Scaini, C. Grunwald, G. Legname, G. Scoles, L. Casalis, Oriented immobilization of prion protein demonstrated via precise interfacial nanostructure measurements, ACS Nano 4 (11) (2010) 6607–6616, http://dx.doi.org/10.1021/nn101872w, PMID: 20958083.

[13] T. Rebetez, SARS-CoV-2 main protease: a kinetic approach, 2022, bioRxiv, URL https://api.semanticscholar.org/CorpusID:248518486.

[14] G. Birarda, D. Bedolla, F. Piccirilli, C. Stani, H. Vondracek, L. Vaccari, Chemical analyses at micro and nano scale at SISSI-Bio beamline at Elettra-Sincrotrone Trieste, in: Z. Huang (Ed.), Biomedical Vibrational Spectroscopy 2022: Advances in Research and Industry, Vol. 11957, International Society for Optics and Photonics, SPIE, 2022, 1195707, http://dx.doi.org/10.1117/12.2607751.

[15] R. Adato, H. Altuga, In-situ ultra-sensitive infrared absorption spectroscopy of biomolecule interactions in real time with plasmonic nanoantennas, Nature Commun. 4 (2013) 2154, http://dx.doi.org/10.1038/ncomms3154.

[16] E. Mirmomtaz, M. Castronovo, C. Grunwald, F. Bano, D. Scaini, A.A. Ensafi, G. Scoles, L. Casalis, Quantitative study of the effect of coverage on the hybridization efficiency of surface-bound DNA nanostructures, Nano Lett. 8 (12) (2008) 4134–4139, http://dx.doi.org/10.1021/nl802722k, PMID: 18983126.

[17] Z. Ganim, K. Jones, A. Tokmakoff, Insulin dimer dissociation and unfolding revealed by amide I two-dimensional infrared spectroscopy, Phys. Chem. Chem. Phys. 12 (2010) 3579–3588, http://dx.doi.org/10.1039/B923515A.

[18] F. Piccirilli, G. Schirò, V. Vetri, S. Lupi, A. Perucchi, V. Militello, Decoding vibrational states of Concanavalin A amyloid fibrils, Biophys. Chem. 199 (2015) 17–24, http://dx.doi.org/10.1016/j.bpc.2015.02.007.

[19] F. Piccirilli, N. Plotegher, F. Spinozzi, L. Bubacco, P. Mariani, M. Beltramini, I. Tessari, V. Militello, A. Perucchi, H. Amenitsch, J. Baldassarri, M. Steinhart, S. Lupi, M.G. Ortore, Pressure effects on α-synuclein amyloid fibrils: An experimental investigation on their dissociation and reversible nature, Arch. Biochem. Biophys. 627 (2017) 46–55, http://dx.doi.org/10.1016/j.abb.2017.06.007.

[20] R. Arya, S. Kumari, B. Pandey, H. Mistry, S. Bihani, A. Das, V. Prashar, G. Gupta, L. Panicker, M. Kumar, Structural insights into SARS-CoV-2 proteins, J. Mol. Biol. 433 (2021) 166725, http://dx.doi.org/10.1016/j.jmb.2020.11.024.